HUNGARIAN JOURNAL OF
INDUSTRY AND CHEMISTRY
Vol. 52(1) pp. 29–35 (2024)
hjic.mk.uni-pannon.hu
DOI: 10.33927/hjic-2024-05

HUNGARIAN JOURNAL OF INDUSTRY AND CHEMISTRY
HJIC

THE ROLE OF TOOL PIN IMPRINTS ON THE MECHANICAL BEHAVIOR OF STRUCTURES REPAIRED USING THE FRICTION STIR WELDING (FSW)TECHNIQUE

HADJ BOULENOUAR HASNA[1], MAZARI MOHAMED[1], BELAZIZ AZZEDDINE[2*], HADJ BOULENOUAR RACHID[3]

1 Laboratory of Materials and Reactive Systems (LMSR), University of Sidi Bel Abbes, 22000, ALGERIA
2 Center of Research in Mechanics, University campus of Chaab Erssas, 73B Freres Ferrad, Constantine, 25017, ALGERIA
3 Laboratory of Mechanics and Physics of Materials (LMPM), Djillali Liabes University, Sidi Bel Abbes, 22000, ALGERIA

Among the various techniques employed to repair structures comprised of materials containing cracks, one of the most prominent is the utilization of friction stir welding (FSW). This method involves a solid-state assembly process. The adoption of FSW as a structural repair technique offers a swift response to meet contemporary industrial demands. When applied to the 5083 H111 aluminum alloy, this technique extended the operational lifespan of components following their repair.

Keywords: friction stir welding (FSW), service life, cracks, repair, tool

1. Introduction

Since the 1990s, friction stir welding (FSW) has been a patented technique applied to aluminum alloys developed by The Welding Institute (TWI) [1]-[2]. This innovative method (*Figure 1*) is highly efficient and particularly useful for welding non-ferrous materials such as copper and aluminum alloys [3]-[4]. Classified among the most frequently used assembly processes, the FSW technique is considered a novel method in the world of assembly [5]-[6]. Although this particular process causes microstructural changes, residual tensions at joints and distortions that are difficult to regulate, it remains a promising technique due to its unique ability to weld parts in the solid state, eliminating defects related to solidification and creating low internal stresses compared to traditional welding methods [7]-[8]. As a result, FSW can be used to join alloys that were previously considered difficult to weld [9]. The principle of FSW is based on the concept of kneading and plasticizing the material using the heat generated by the friction between the tool and the parts to be welded, which are held rigidly to prevent any movement during this process [10]. A multitude of process parameters - including the rotational speed, velocity and angle of inclination of the tool as well as the depth to which the tool is immersed - have a direct impact on the quality of the final product obtained thanks to FSW [11]. In addition, other parameters can influence the final properties of FSW seals [12]-[13]. Many unique properties of aluminum alloys, in particular their lightness and good structural strength, allow them to be used in structural components [14]. Aluminum alloys meet the needs of the aerospace and automotive industries for lightweight materials [15]. The aluminum alloys AA6XXX and AA5XXX are commonly used in the manufacture of aircraft structures and in other structural applications [15]. Several studies of FSW with regard to various AA5XXX and AA6XXX joints have been reported in the literature [16]. Shigematsu et al. [17] attempted an FSW assembly of alloys AA5083 and AA6061 with different thicknesses, moreover, studied the microstructure and mechanical properties of the joints. Peel et al. [18] studied the processing window of 3 mm-thick AA5083 and AA6082 joints and found that the rotational speed of the tool affected heat generation during welding more than the feed rate. Peel et al. [18] studied the effects of the rotation and velocity of the tool on the microstructure, hardness and distribution of the precipitates of 3-mm thick AA5083 and AA6082 joints. Steuwer et al. [19] quantified the effects of tool rotation and velocities on the residual stress in 3 mm-thick AA5083 and AA6082 joints. He concluded that the

Received: 16 Nov 2023; Revised: 11 Jan 2024;
Accepted: 24 Jan 2024
*Correspondence: belaziz2013@gmail.com

rotational speed of the tool is a useful process variable to minimize residual stresses. In this work, an attempt was made to produce an AA5083 H111 aluminum alloy using FSW and study the influence of the tool pin imprint on delaying crack propagation in an aluminum alloy welded by FSW.

2. Experimental study

The analysis was carried out experimentally in the laboratory of materials and reactive systems using an Instron machine driven by a servo hydraulic actuator with a capacity of 50 kN and 100 kN in static and dynamic modes, respectively (*Figure 2*). The FSW process was carried out on a modified conventional milling machine in the workshop of the mechanical engineering department at Djillali Liabes University of Sidi Bel Abbes.

2.1. Material studied

The material studied was an aluminum alloy of the 5000 series, type 5083 in the H111 condition (25% deformed by rolling). The alloy 5083 H111 was chosen because the proportions of magnesium and manganese quite closely resemble those of the 2024 alloy used in aeronautical structures of fuselages. Its chemical composition and characteristics are given in *Table 1* [21] where *E* – elastic modulus, *YS* -yield strength, *UTS* – ultimate tensile strength, *A* - elongation, *HV* – Vickers hardness, *KI* – stress intensity factor.

2.2. Tensile test

The mechanical characteristics of the alloy studied were determined by a tensile test carried out on a dumbbell specimen (*Figure 3*) [22].

A tensile test was performed using extensometers. The machine was controlled in accordance with a standard at a velocity of 20 mm/min and an initial load of 1 kN. The traction curve of this test is represented in *Figure 4*.

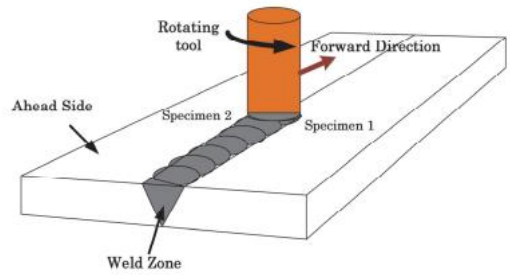

Figure 1: Schematic diagram of the FSW process [20]

Figure 2: Instro machine used for traction

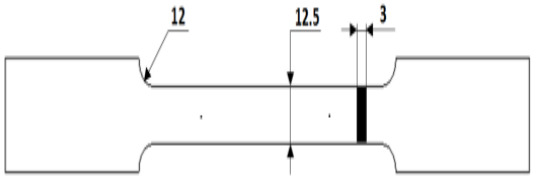

Figure 3: Geometry of the dumbbell specimen [22]

Table 1: Plant material characteristics: Aluminum Alloy 5083 H111 [21]

Al	Si	Fe	Cr	Mn (%)	Mg	Cr	Zn	Ti
0.15	0.40	0.40	0.10	0.10	4.90	0.25	0.25	0.15

E (MPa)	*Ys* (MPa)	*UTS* (MPa)	*A* (%)	*HV*	*KI* (J/Cm^2)
71008	155	236	16.5	88	45

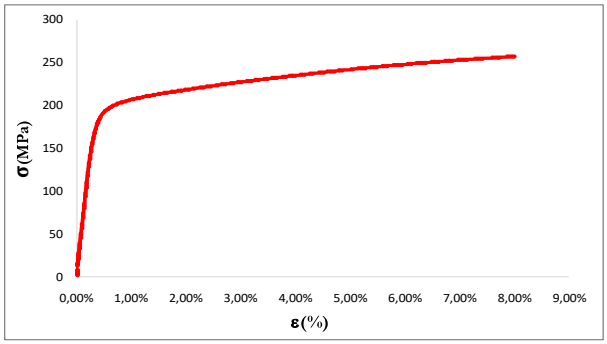

Figure 4: Tensile curve of aluminium alloy 5083 H111 in the Longitudinal L direction

Table 2: Mechanical characteristics of alloy 5083 H111

E (MPa)	*Ys* (MPa)	*UTS* (MPa)	*A* (%)	*HV*
49891	175	250	8	138

Dumbbell-shaped specimens of the relevant material were extracted (*Figure 5*) by following the ASTM E8-04 standard [23], which includes a calibrated central section with a cross sectional area of S=400 mm^2 and a length of L=200 mm. The tensile tests were conducted at room temperature.

Table 2 illustrates the main mechanical characteristics obtained.

2.3. Fatigue test

In this study, CT75 specimens in the aluminum alloy 5 mm thick (B) and 75 mm wide (W) (*Figure 6*) were used according to the ASTM E647-00 standard [24].

2.4. Description and analysis of the tests

All the tests were performed under constant amplitude loading with the stress applied ranging from 26 to 42 MPa. Some trials were stopped before the specimens broke.

Test No. 1:

During this test, initiation took place at 36270 cycles. The maximum load (σ_{max}) applied was 2500 N with a load ratio (R) of 0.1.

The crack extended to 26.7 mm in length before rupturing, which corresponds to 229270 cycles (*Figure 7*).

Test No. 2:

Initiation took place at 40000 cycles. The applied σ_{max} was 2500 N, R = 0.1.

The crack extended to 26.7 mm in length before rupturing, which corresponds to 217000 cycles (*Figure 8*).

Figure 9 represents the results obtained for the two specimens regarding the length of the crack as a function of the number of cycles (N). It can be seen that the two results exhibit the same trend and are similar.

Propagation rates:

To compare the change in cracking rate in the case of the two specimens (*Figure 10*), the seven-point method was applied from the experimental data points to obtain a linear regression.

For both specimens, the propagation speed (da/dN) changed as a function of the amplitude of the stress intensity factor (ΔK) following the same trend and obeying the Paris' law:

$$\frac{da}{dN} = A(\Delta K)^m \quad (1)\ [25]$$

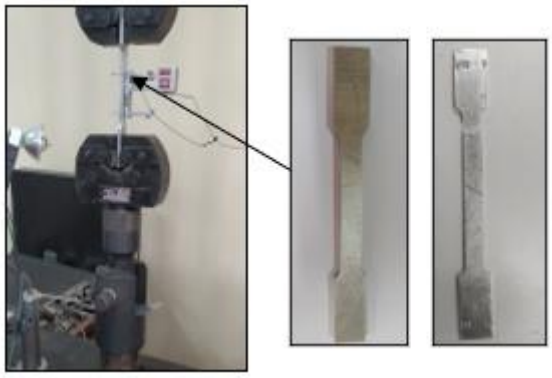

Figure 5: Set-up of the tensile test

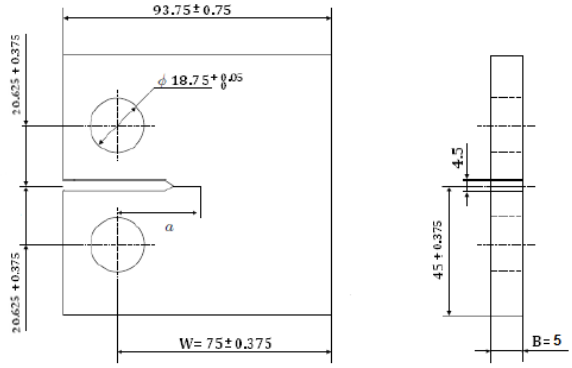

Figure 6: Dimensions of the CT75 specimens

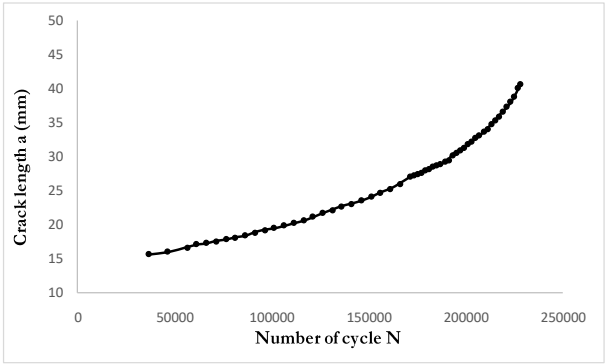

Figure 7: Change in crack length (a) as a function of the number of cycles (N) when ΔP was constant (Test No.1)

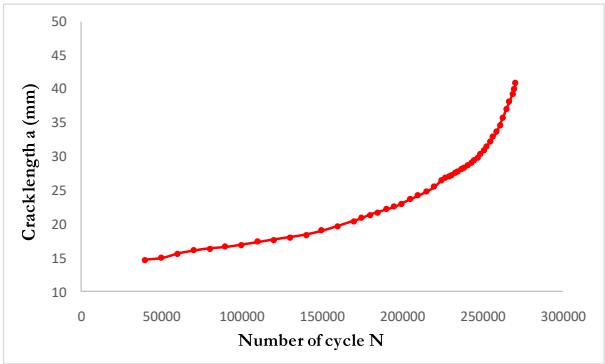

Figure 8: Change in the crack length (a) as a function of the number of cycles (N) when ΔP was constant (Test No.2)

Table 3: Coefficients and exponents of the Paris' law

Specimen	*da/dN* (mm/cycle)	ΔK (MPa·m$^{1/2}$)
1	$3x10^{-7}\Delta K^{2.60}$	7 to 17
2	$2x10^{-7}\Delta K^{2.87}$	7 to 15

where *A* and *m* refer to two characteristic constants of the material.

Table 3 represents the results obtained for the two specimens.

It is noteworthy that the *da/dN* values for the two specimens are almost identical.

2.5. Welding operation

To carry out a friction stir welding operation, the mechanical action of the tool on the part is important. The welding energy is purely mechanical and essentially corresponds to the work of the torque. The significant forces applied by the tool on the parts to be welded require the use of positioning and holding systems [26].

The heat generated by the friction between the shoulder and the pin transforms the material into a pasty state in the vicinity of the tool, moreover, facilitates the penetration and movement of the tool along the joint to be welded to form the weld after cooling [26].

2.6. Welding tool

Generally speaking, the welding tool is cylindrical, consisting of a profiled pin and a shoulder. The welding cycle begins with a sequence of penetrations of the rotating pin into the plates to be welded. The shoulder resting against the parts allows the material it will contain to flow [27]-[28].

The tool used was made in the mechanical manufacturing workshop of the Mechanical Engineering Department at Djillali Liabes University of Sidi Bel Abbes from the alloy tool steel Z200C12 (*Figure 11*):

Nowadays, Z200C12 steel, along with its derivatives, constitutes one of the first families of tool steel, both in terms of the importance of the tonnages used each year and the extraordinarily diverse range of its applications. However, despite the long-established and widespread use of its steels, users still sometimes encounter serious difficulties with its implementation, particularly regarding its heat treatment [29].

Figure 12 depicts the FSW processing and the FSW tool.

2.7. Machine used for FSW

The FSW welding process was carried out on a modified conventional milling machine in the workshop of the Mechanical Engineering Department.

Before the FSW process, a good clamping system had to be made. By clamping it down with a stepped test piece, this technique positioned the test piece on an anvil fixed to the table to avoid the part from separating when

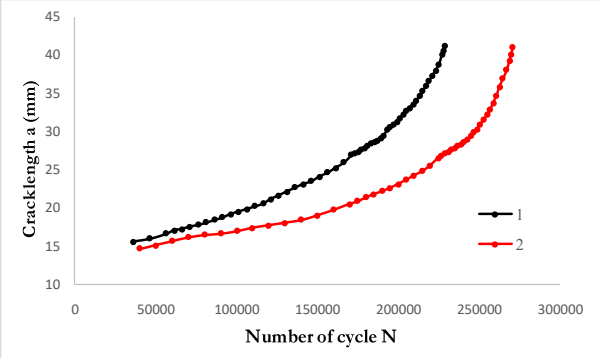

Figure 9: Results of the fatigue tests regarding the crack length of the aluminum alloy 5083 H111 as a function of the number of cycles (*N*)

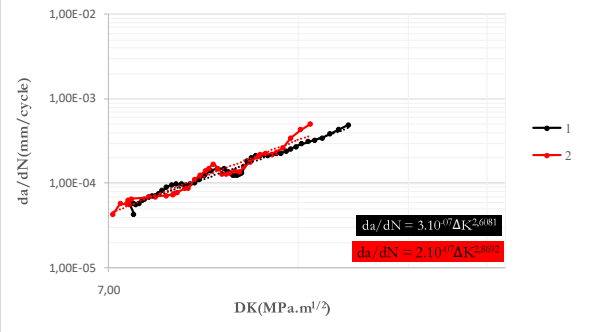

Figure 10: Change in the cracking rate as a function of ΔK

Figure 11: Manufacturing of the tool

Figure 12: FSW welding tool

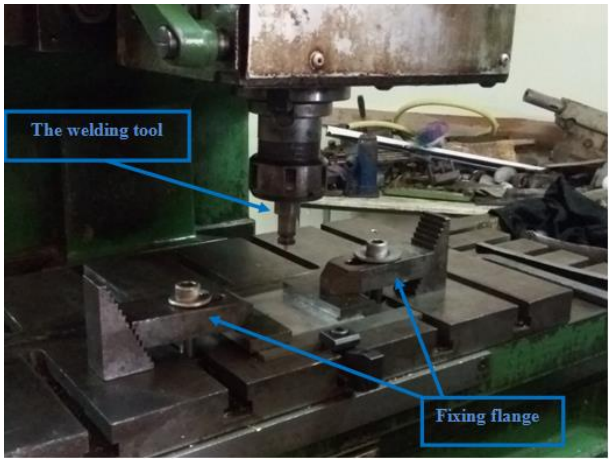

Figure 13: Clamping mode

the tool penetrates it. *Figure 13* represents the clamping mode used.

2.8. The welding parameters

In this process, a non-standardized tool geometry relative to the thickness of the specimen was used to obtain an imprint with a small diameter. Several tests were carried out to obtain the right parameters that result in a good weld seam, which are as follows:

- Feed speed (Va) = 160 m/min
- Rotational speed (v) = 2000 rpm
- Angle of inclination (θ) = 1.5°

The indentation tests were conducted in the LMSR laboratory (*Figure 14*).

Figure 14: The CT75 specimens after welding

Two methods were used for welding: firstly, welding took place outwards to avoid traces of the imprint on the zone to be welded; and secondly, inwards to leave the imprint.

2.9. Welded specimen without an imprint

After the welding step, the fatigue tests on the two specimens were replicated.

During this test, initiation took place at 70000 cycles. The applied σ_{max} was 2500 N with R = 0.1.

The crack extended to 29.6 mm in length before rupturing, which corresponds to 279500 cycles (*Figure 15*).

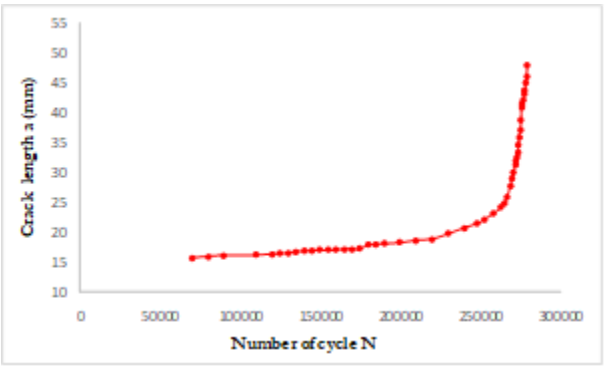

Figure 15: Change in crack length as a function of the number of cycles (N) when ΔP was constant

2.10. Welded specimen with an imprint

During this test, initiation took place at 85000 cycles. The applied σ_{max} applied was 2500 N with R = 0.1.

The crack extended to 29.6 mm in length before rupturing, which corresponds to 641600 cycles (*Figure 16*).

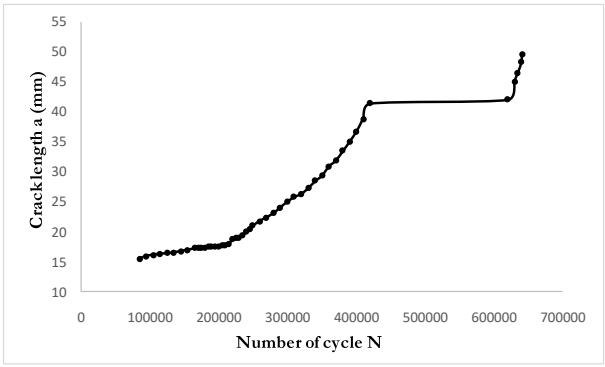

Figure 16: Change in crack length (a) as a function of the number of cycles (N) when ΔP was constant

Figure 17 represents the results obtained for the two specimens after welding regarding the length of the crack as a function of the number of cycles after welding. It can be seen that in the specimen with the imprint, the delay in the propagation of the cracks (N_d) is equal to

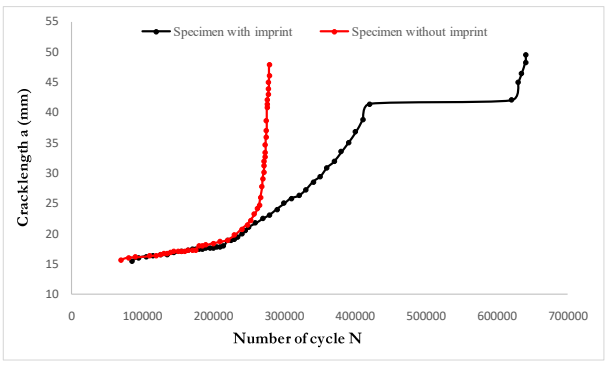

Figure 17: Results of the fatigue tests on the aluminum alloy 5083 H111 regarding the crack length (a) as a function of the number of cycles (N)

approximately 2.2x10^5, which is significant since it clearly shows the influence of the imprint of the tool pin on the propagation of the crack.

2.11. Propagation rates

The tests concerning the propagation rate of the fatigue cracks were carried out on both specimens after welding (*Figure 18, Table 4*).
3 zones were identified:

- Zone A corresponds to the area where the crack initiated;
- Zone B represents the domain of Paris (the quasi-linear curve illustrating continuous propagation of the cracks).
- Zone C refers to the imprint of the pin of the tool. This phenomenon is characterized by a fairly significant delay (N_d) of 220,000 cycles before the crack continued to lengthen.

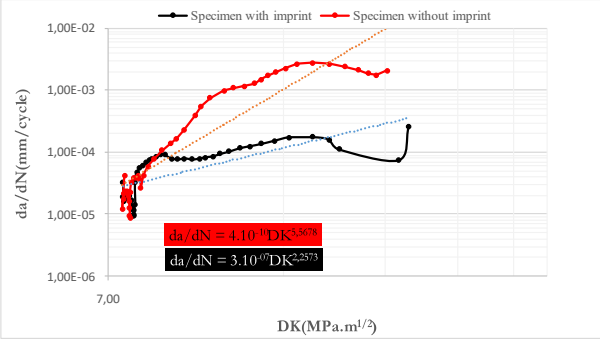

Figure 18: Change in cracking rate as a function of ΔK

Table 4: Coefficients and exponents of the Paris' law regarding the two specimens after welding

Specimen	*da/dN* (mm/cycle)	*ΔK* (MPa·m$^{1/2}$)
without an imprint	$4x10^{-10}\Delta K^{5.57}$	7 to 22
with an imprint	$3x10^{-7}\Delta K^{2.26}$	7 to 24

2.12. Validation

Our results, presented in *Figure 16*, are consistent with those recorded in a study by H. Wu (*Figure 19*) [30], which digitally simulated the propagation of fatigue cracks after the cracked structures had been repaired by drilling a centered hole or crack bottom on aluminum alloys 6082T6 and 5083H111, respectively.

3. Conclusion

This experimental study dealt with the influence of an imprint on delaying the propagation of fatigue cracks. The results obtained show that instead of being regarded as a defect, the imprint of the tool has become an additional means of delaying the propagation of cracks and, therefore, a means of their repair, which may be worthy of further study.

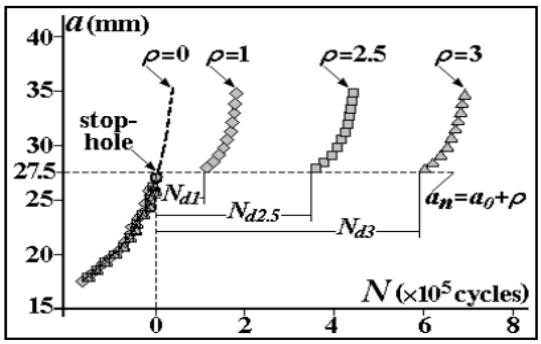

Figure 19: The typical effect of the hole on the propagation of the fatigue crack [30]

REFERENCES

[1] Fu. Z.-H.; He, D.-Q.; Wang, H.: Friction stir welding of aluminum alloys, *J. Wuhan Univ. Technol. Mater. Sci. Ed.*, 2004, **19**(1), 61–64, DOI: 10.1007/bf02838366

[2] Vivas, J; Fernández-Calvo, A.-I.; Aldanondo, E.; Irastorza, U.; Álvarez, P.: Friction stir weldability at high welding speed of two structural high pressure die casting aluminum alloys, *J. Manuf. Mater. Process.*, 2022, **6**(6), 160, DOI: 10.3390/jmmp6060160

[3] Heidarzadeh, A.; Mironov, S.; Kaibyshev, R.; Cam, G.; Simar, A.; Gerlich, A.; Khodabakshi, F.; Mostafaei, A.; Field, D.P.; Robson, J.D.; Deschamps, A.; Withers, P.J.: Friction stir welding/processing of metals and alloys: A comprehensive review on microstructural evolution, *Prog. Mater. Sci.*, 2021, **117**, 100752, DOI: 10.1016/j.pmatsci.2020.100752

[4] Olakanmi, E.O.; Cochrane, R.F.; Dalgarno, K.W.: A review on selective laser sintering/melting (SLS/SLM) of aluminium alloy powders: Processing, microstructure, and properties, *Prog. Mater. Sci.*, 2015, **74**, 401–477, DOI: 10.1016/j.pmatsci.2015.03.002

[5] Rabe, P.; Reisgen, U..; Schiebahn, A.: Non-destructive evaluation of the friction stir welding process, generalizing a deep neural defect detection network to identify internal weld defects across different aluminum alloys, *Weld. World*, 2023, **67**, 549–560, DOI: 10.1007/s40194-022-01441-y

[6] El-Sayed, M.M.; Shash, A.Y.; Abd-Rabou, M.; ElSherbiny, M.G.: Welding and processing of metallic materials by using friction stir technique: A review, *J. Adv. Join. Processes*, 2021, **3**, 100059, DOI: 10.1016/j.jajp.2021.100059

[7] Norouzian, M.; Elahi, M.A.; Plapper, P.: A review: Suppression of the solidification cracks in the laser welding process by controlling the grain structure and chemical compositions, 2023, **7**, 100139, DOI: 10.1016/j.jajp.2023.100139

[8] Kah, P.; Rajan, R..; Martikainen, J.; Suoranta, R.: Investigation of weld defects in friction-stir welding and fusion welding of aluminium alloys, *J. Mater. Sci.: Mater. Eng.*, 2015, **10**, 26, DOI: 10.1186/s40712-015-0053-8

[9] Heidarzadeh, A.; Mironov, S.; Kaibyshev, R.; Cam, G.; Simar, A.; Gerlich, A.; Khodabakhshi, F.; Mostafaei, A.; Field, D.P.; Robson, J.D.; Deschamps, A.; Withers, P.J.: Friction stir welding /processing of metals and alloys: A comprehensive review on microstructural evolution, *Prog. Mater. Sci.*, 2021, **117**, 100752, DOI: 10.1016/j.pmatsci.2020.100752

[10] Geiger, M.; Micari, F.; Merklein, M.; Fratini, L.; Contorno, D.; Giera, A.; Staud, D.: Friction stir knead welding of steel aluminium butt joints, *Int. J. Mach. Tools Manuf.,* 2008, **48**(5), 515–552, DOI: 10.1016/j.ijmachtools.2007.08.002

[11] Emamian, S.S.; Awang, M.; Yusof, F.; Sheikholeslam, S.; Mehrpouya, M.: Improving the friction stir welding tool life for joining the metal matrix composites, *Int. J. Adv. Manuf. Technol.*, 2020, 106, 3217–3227, DOI: 10.1007/s00170-019-04837-1

[12] He, X.; Gu, F.; Ball, A.: A review of numerical analysis of friction stir welding, *Prog. Mater. Sci.,* 2014, **65**, 1–66, DOI: 10.1016/j.pmatsci.2014.03.003

[13] Shanmughasundaram, P.; Dahle, A.K.: Heat treatment of aluminum alloys, *Ref. Module Mater. Sci. Mater. Eng.*, 2018, DOI: 10.1016/B978-0-12-803581-8.03374-9

[14] Sankaran, K.K.; Mishra, R.S.: Chapter 4 - Aluminum alloys, in: Mettallurgy and Design of Alloys with Hierarchical Microstructures; Sankaran, K.K.; Mishra, R.S. (Elsevier), 2017, pp. 57–176, DOI: 10.1016/B978-0-12-812068-2.00004-7

[15] Zheng, K.; Politis, D.J.; Wang, L.; Lin, J.: A review on forming techniques for manufacturing lightweight complex-shaped aluminium panel components, *Int. J. Lightweight Mater. Manuf.*, 2018, **1**(2), 55–80, DOI: 10.1016/j.ijlmm.2018.03.006

[16] A, S.S.; Kumar, A.; Mugada, K.K.: Investigation of material flow, microstructure evolution, and texture development in dissimilar friction stir welding of Al6061 to Ti6Al4V, *Mater. Today Commun.*, 2022, **33**, 104424, DOI: 10.1016/j.mtcomm.2022.104424

[17] Kwon, Y.J.; Shigematsu, I.; Saito, N.: Dissimilar friction stir welding between magnesium and aluminum alloys, *Mater. Lett.*, 2008, **62**(23), 3827–3829, DOI: 10.1016/j.matlet.2008.04.080

[18] Peel, M.J.; Steuwer, A.; Withers, P.J.: Dissimilar friction stir welds in AA5083-AA6082. Part II: Process parameter effects on microstructure, *Metall. Mater. Trans. A Phys Metall. Mater. Sci.*, 2006, **37**(7), 2195–2206, DOI: 10.1007/BF02586139

[19] Steuwer, A.; Peel, M.J.; Withers, P.J.: Dissimilar friction stir welds in AA5083-AA6082: The effect of process parameters on residual stress, *Mater. Sci. Eng. A*, 2006, **441**(1-2), 187–196, DOI: 10.1016/j.msea.2006.08.012

[20] Khansari, N.M.; Betro, F.; Karimi, N.; Ghoreishi, S.M.N.; Fakoor, M.; Mokari, M.: Development of an optimal process for friction stir welding based on GA-RSM hybrid algorithm, *Frat. Integrita Strutt.*, 2018, **12**(44), 106–122, DOI: 10.3221/IGF-ESIS.44.09

[21] Bounini, B.T.; Bouchouicha, B.; Ghazi, A.: Simulation of the behavior of aluminium alloys welded friction stir welding FSW (Case of AA5083 and AA 6082), *Frat. Integrita Strutt.*, 2018, **12**(46), 1–13, DOI: 10.3221/IGF-ESIS.46.01

[22] Belaziz, A.; Mazari, M.; Medjadji, A.: Effect of the hole expansion technique on the crack propagation delay, Sidi Bel Abbes University, Algeria, *13th Mechanics Congress*, 2017, 11–14

[23] American Society for Testing and Materials ASTM E8-04 (2003): Standard Test Methods for Tension Testing of Metallic Materials, 03(01), Metals Mechanical Testing Elevated and Low Temperature Tests Metallographic, 2003

[24] ASTM Standard E647-00, Standard Test Method for Measurement of Fatigue Crack Growth, 03(01), Metals Mechanical Testing Elevated and Low Temperature Tests Metallographic, 2003

[25] Dong, J.; Pei, W.; Ji, H.; Long, H.; Fu, X.; Duan, H.: Fatigue crack propagation experiment and numerical simulation of 42CrMo steel, *Proc. Inst. Mech. Eng. C J. Mech. Eng. Sci.*, 2020, **234**(14), 2852–2862, DOI: 10.1177/0954406220910458

[26] Khalafe, W.H.; Sheng, E.L.; Bin Isa, M.R.; Omran, A.B.; Shamsudin, S.B.: The effect of friction stir welding parameters on the weldability of aluminum alloys with similar and dissimilar metals: Review, *Metals*, 2022, **12**(12), 2099, DOI: 10.3390/met12122099

[27] Sunnapu, C.; Kolli, M.: Tool shoulder and pin geometry's effect on friction stir welding: A study of literature, *Mater. Today: Proc.*, 2021, **39**, 1565–1569, DOI: 10.1016/j.matpr.2020.05.601

[28] Kocsisné Pfeifer, É.; Mink, J.; Gyurika, I.G.; Telegdi, J.: Effect of heat treatment on the structure of self-assembled undecenyl phosphonic acid layers developed on different stainless steel surfaces, *Hung. J. Ind. Chem.*, 2023, **51**(2), 7–14, DOI: 10.33927/hjic-2023-12

[29] Alioui, S.; Himour, A.: Effect of heat treatment on friction and wear behavior of Ni-based thermal spray coating deposited on Z200C12 steel, *Mater. Res. Express*, 2019, **6**(12), 126563, DOI: 10.1088/2053-1591/ab58f0

[30] Wu, H.: Residual fatigue cracked structures after repair by the hole method. *CFM 2009 – 19th French Congress of Mechanics*, 2009